

Syngas Segregation Induced by Confinement in Carbon Nanotubes: A Combined First-Principles and Monte Carlo Study

Jing Guan,[†] Xiulian Pan,^{*,†} Xin Liu,[‡] and Xinhe Bao^{*,†}

State Key Laboratory of Catalysis, Dalian Institute of Chemical Physics, Chinese Academy of Sciences, Dalian 116023, China, and Department of Chemistry, Dalian University of Technology, Dalian 116024, China

Received: June 29, 2009; Revised Manuscript Received: October 20, 2009

A theoretical study combining first-principles and Monte Carlo simulations has been carried out to investigate the interactions of H₂ and CO molecules with carbon nanotube (CNT) surfaces. The results show that there are stronger interactions of both H₂ and CO with the interior nanotube surface than with the exterior surface. In addition, CO interacts more strongly with CNT surfaces than H₂. This can be explained by the nature of the molecules and the different electronic properties of the concave and convex surfaces of CNTs formed by graphene layers. As a result, syngas molecules are enriched inside CNTs and the enrichment generally becomes greater in smaller nanotubes. Furthermore, the ratio of CO/H₂ inside CNTs increases with respect to the composition of syngas in the exterior gas phase. The enriched reactants and altered CO/H₂ ratio inside nanotubes could be beneficial for the reaction rate and lead to modification of the product selectivity.

1. Introduction

Carbon nanotubes (CNTs) have attracted wide interest owing to their unusual structural, electronic, and mechanical properties.^{1–3} Typical CNTs have diameters ranging from less than 1 to 100 nm, which enables the encapsulation of a variety of substances in the interior cavity. For example, fullerene and its derivatives, water, alkali metals, and halides, have been introduced inside CNT channels and some structural properties of these substances have been reported to be modified due to confinement.^{4–7} We observed that the reduction of transition metal oxide nanoparticles is facilitated while the oxidation of metallic particles is retarded when they are confined inside CNTs.^{8,9} Furthermore, Rh–Mn nanoparticles confined inside CNT channels exhibit an enhanced activity for catalyzing the conversion of syngas (a mixture of CO and H₂) to oxygenates compared to those located on the more accessible exterior surfaces of CNTs.¹⁰ Similarly, CNT-confined iron also exhibits a higher activity in Fischer–Tropsch synthesis than the outside iron catalyst.¹¹ We proposed there that the modification of redox properties of metal nanoparticles due to interaction with the graphene walls likely play an important role in these composite materials in addition to the spatial restriction within CNT channels, which could limit sintering of metal particles and affect diffusion of reactants and products.¹²

Furthermore, inside such small CNT channels the interactions of gas molecules with the graphene layers may also become increasingly important and finally dominate in comparison to the intermolecular interactions.¹³ They could be strong enough to influence the transport and distribution of reactant molecules inside CNTs, which may affect the reaction rate and selectivity. Therefore we intend to investigate the local concentrations of syngas molecules inside and outside of CNTs here, moving toward a more detailed understanding of the important effects during syngas conversion over metal catalysts confined inside

CNTs. As a start, we look into the interactions of syngas molecules with CNT surfaces in the absence of metal catalysts.

The adsorption isotherms of gases such as H₂, N₂, O₂, and Ar on CNTs have been studied earlier using Monte Carlo simulations,^{14–16} but no distinction was made between the interior and exterior sides of CNTs, and the potential functions of planar graphite layer were generally used. However, it is known that there is charge redistribution and polarization in curved surfaces of CNTs,^{7,17,18} which could cause differences in the physisorption of molecules because of electrostatic forces and van der Waals interactions. For example, using density functional theory molecules such as H₂, CF₄, and 1-heptene have been found to exhibit different binding strengths on the interior and exterior graphene surfaces.^{4,19–24} In particular, the adsorption of H₂ has been widely studied since the 1990s because H₂ is a promising clean alternative fuel and CNTs are considered as a potential material for hydrogen storage.^{25,26} In contrast, the adsorption of CO was seldom studied. Although Gu et al. simulated the separation of CO and H₂ mixture using single-walled CNT (SWNT) bundles as a sorbent, potentials of the graphite were used and the interior and exterior CNT surfaces were not distinguished.²⁷ Here we first studied the interaction of CO and H₂ with both the interior and exterior surfaces of CNTs and obtained their interaction potential parameters from first-principles calculations. Then the local distributions of CO and H₂ inside and outside of CNTs were calculated with Monte Carlo simulations when CNTs were placed in a syngas atmosphere (CO/H₂ = 0.5).

2. Computational Details

2.1. First Principles Calculations. First-principles calculations were performed with the Gaussian98 software package.²⁸ We used second-order Møller–Plesset perturbation theory (MP2) to calculate the H₂–CNT and CO–CNT binding energies since this method is known to be more suitable for description of long-range dispersion forces than conventional density functional theory.^{29–31} The size of the cluster model and basis set were determined by comparing the binding energies of H₂ on a planar graphite layer with those obtained by a more accurate

* To whom correspondence should be addressed. Tel: +86-411-84686637. Fax: +86-411-84694447. E-mail: (X.B.) xhbao@dicp.ac.cn; (X.P.) panxl@dicp.ac.cn.

[†] Chinese Academy of Sciences.

[‡] Dalian University of Technology.

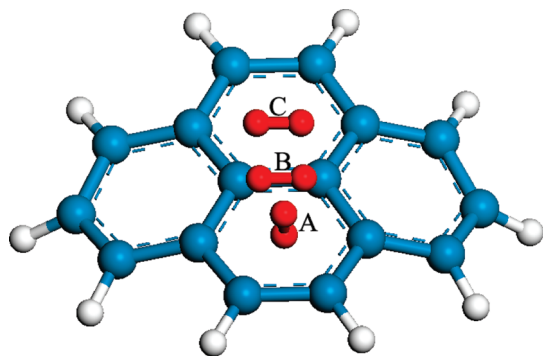


Figure 1. A curved pyrene $C_{16}H_{10}$ cluster model, where the terminal atoms are saturated with H atoms. The blue and light gray spheres denote C and H atoms, respectively. The molecules (red spheres) approach the CNT surface in three different orientations (A, hollow site at the center of a hexagonal carbon ring; B, bridge site parallel to the C–C bond of the nanotube; and C, surface site parallel to a hexagonal carbon ring of the CNT surface).

MP2/aug-cc-PVTZ method.³⁰ As shown in Figure S1 of Supporting Information, we took the basis set 6-311++g (2d, p) as an optimum compromise considering the computational time and accuracy.

A pyrene $C_{16}H_{10}$ cluster was used to model a CNT here since the adsorbed molecules mainly interact with the neighboring carbon atoms (Figure 1). Similar cluster models have been used for graphene layers and CNTs in earlier studies.^{30,31} The concave surface of the bent pyrene mimics the interior CNT while the convex surface represents the exterior nanotube surface. The pyrene curvature was adjusted to match that of CNTs with different diameters. All the dangling bonds at the tube ends were saturated with hydrogen atoms placed along the C–C bonds at a distance of 1.084 Å. The bond lengths of molecules and the C–C distances in the nanotube wall were frozen and only the molecule–CNT distances were allowed to vary. We first identified the most stable adsorption sites for both H_2 and CO on CNT surfaces (Figure 1). Their binding energies were compared with that on graphite (E_b^{graphite}):

$$x^{\text{in(ext)}} = [E_b^{\text{in(ext)}} - E_b^{\text{graphite}}] / E_b^{\text{graphite}} \quad (1)$$

The potential parameters of H_2 and CO on the interior and exterior CNT surfaces $\epsilon^{\text{in(ext)}}$ were obtained according to eq 2 and listed in Table 1. The cross-interaction parameters $\epsilon^{\text{graphite}}$ for H_2 (CO)–graphite were taken from earlier studies and shown in Table S1 of the Supporting Information.^{32,33}

$$\epsilon^{\text{in(ext)}} = [1 + x^{\text{in(ext)}}] \times \epsilon^{\text{graphite}} \quad (2)$$

2.2. GCMC Simulations. The distribution of molecules inside and outside of CNT channels were calculated with Monte Carlo simulations using the interaction potential parameters obtained from first-principles calculations. The intermolecular interactions were modeled by the site–site Lennard-Jones (LJ) potential (eq 3).

$$U_i = 4\epsilon[(\sigma/r_i)^{12} - (\sigma/r_i)^6] \quad (3)$$

Instead of simulating CO by a structureless single-spherical site,²⁷ we used a two-site LJ model (denoted as 2LJ) with two LJ spheres separated by a distance of 1.14 Å. The potential parameters for the well depth and collision diameter of C and O atoms were adopted from the study of Piper et al.³⁴ The interatomic CO–graphite interaction was modeled using the LJ potentials, which were reproduced from the experimentally determined CO–graphite adsorption data by Steele et al.³² We

also compared a 3LJ model reported by Straub and Karplus,³³ which considered dipole and quadrupole characteristics of the CO molecule. CO was represented as three-site LJ spheres with partial negative charges on C ($q_C = -0.75e$) and O ($q_O = -0.85e$) atoms, and a positive charge $q_{\text{COM}} = 1.6e$ at its massless center-of-mass (COM) to maintain electroneutrality. Meanwhile, H_2 was treated as a diatomic molecule with a bond length of 0.74 Å.¹⁵ Table S2 in Supporting Information lists the LJ potential parameters of H, C, and O atoms for both 2LJ and 3LJ models. Figure S2 in Supporting Information shows that the potential energy surfaces (defined by U_i in eq 3) of H_2 and CO on the (10, 10) CNT calculated using the potential parameters from the 2LJ model (Table 1) were much closer to the ab initio binding energy curves with respect to those predicted from the 3LJ model. Therefore, we employed the 2LJ model in the following simulations.

GCMC simulations were carried out with Sorption software, CERIU2 (version 4.2) of MSI.³⁵ Ideal gas behavior was assumed for H_2 and CO in the bulk and the chemical potentials in the adsorbed phase were considered to be the same as those in the gas phase. Because only one set parameters can be assigned to a CNT in this software package, we had to employ a double-walled CNT (DWNT) model, for example, (10, 10)–(13, 13). The distance between the two walls was small enough (2.04 Å) to exclude entry of any molecules in the gap. The potential parameters of the exterior (10, 10) surface obtained above were used to model the outside (13, 13) tube, while those of the interior (10, 10) surface were used for the inside (10, 10) tube for simplicity of calculation.³⁶ We analyzed the influence of the exterior (10, 10) potentials on the interactions between the molecule and exterior (13, 13) surface and found that this could be neglected (Figure S3 in Supporting Information). So could the interior (13, 13) potentials on the interactions of molecules–interior (10, 10) surface be neglected.

Such a DWNT was placed in a rectangular box ($66.5 \times 66.5 \times 24.4 \text{ \AA}^3$), which was aligned periodically in three dimensions, as shown in Figure 2. The space between the neighboring tube walls was set at approximately 50 Å so that the interaction between tubes can be neglected. The space from the outer rim of the CNT to the perimeter of this simulation box was considered to be the exterior volume of the CNT and amounted to $1 \times 10^5 \text{ \AA}^3$ for (10, 10)–(13, 13) DWNT. Periodic boundary conditions were imposed in all three dimensions and the CNT was treated as rigid.

The GCMC simulations consisted of 3×10^7 steps for each state point. The system reached a thermodynamic equilibrium after 1.5×10^7 steps and the molecule distributions were calculated by averaging those within the following 1.5×10^7 steps. The inside and outside concentrations were defined as the equilibrium numbers of molecules divided by the volume of the CNT channel and the exterior volume, respectively. The effects of pressure and temperature, as well as CNT diameters were studied. The partial pressure ratio of CO/ H_2 was fixed at 0.5 in the gas phase, which is the composition frequently used in experimental studies.^{11,12}

3. Results and Discussion

3.1. Interactions of CO and H_2 Molecules with CNTs.

Three adsorption sites were considered on the CNT surfaces, as shown in Figure 1. They are (A) the hollow site at the center of a hexagonal carbon ring with the molecule axis oriented perpendicular to the CNT surface, (B) the bridge site with the molecule oriented parallel to the C–C bond of the CNT surface and (C) the surface site with the molecule sitting above a

TABLE 1: LJ Potential Parameters of H₂ and CO Molecules Interacting with a (10, 10) CNT^a

model	exterior (10, 10)						interior (10, 10)					
	ϵ_{CS}/k_B (K)	σ_{CS} (Å)	ϵ_{OS}/k_B (K)	σ_{OS} (Å)	ϵ_{HS}/k_B (K)	σ_{HS} (Å)	ϵ_{CS}/k_B (K)	σ_{CS} (Å)	ϵ_{OS}/k_B (K)	σ_{OS} (Å)	ϵ_{HS}/k_B (K)	σ_{HS} (Å)
2LJ	31.6	3.39	37.3	3.14	30.7	3.18	42.5	3.39	50.3	3.14	37.6	3.18

^a The subscript “s” stands for the interactions between CNT C–C.

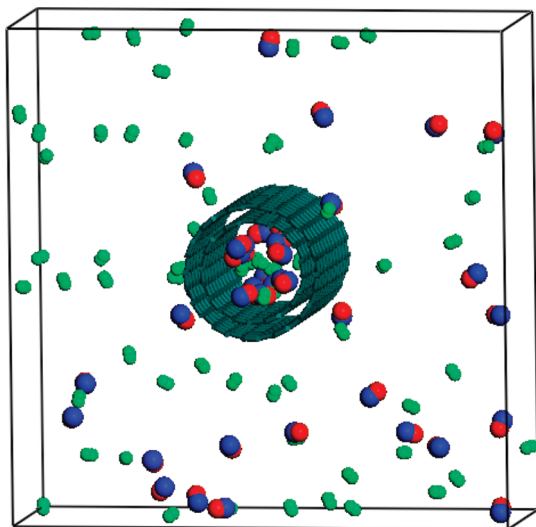


Figure 2. Simulation model of a (10, 10)-(13, 13) DWNT placed in a box of $(66.5 \times 66.5 \times 24.4 \text{ Å}^3)$, which was aligned periodically in three dimensions. The molecules with blue and red spheres represent CO and the light green spheres for H₂.

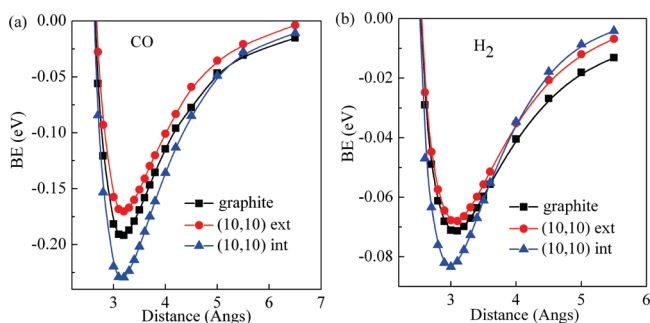


Figure 3. The MP2 binding energies of (a) CO and (b) H₂ on the most stable sites of (10, 10) CNT surfaces in comparison to that on a planar graphite layer as a function of the distance between the center of the adsorbed molecule and CNT surfaces.

hexagonal carbon ring and the molecular axis oriented parallel to the surface. We first took the (10, 10) CNT as an example and calculated the CO–CNT and H₂–CNT binding energies at the MP2 level. Figure 3 shows the binding energy curves for the most favorable adsorption sites as a function of the distance L between the center of the adsorbed molecule and CNT surfaces in comparison with that on a planar graphite layer. Figure S4 of Supporting Information displays the curves for less stable adsorption sites on both interior and exterior surfaces of CNTs. Table 2 summarizes the equilibrium distance L and the corresponding binding energy on different sites.

On the exterior CNT surface, site B is the most favorable for CO adsorption, followed by sites C and A. On site A, CO adsorption takes place with the C atom pointing toward the CNT surface with an equilibrium distance of 3.6 Å. The binding energy E_b is -0.124 eV , consistent with the value (-0.131 eV) reported for the same configuration at $L = 3.4 \text{ Å}$ using DFT within the local density approximation (LDA).³⁷ In comparison,

TABLE 2: The Equilibrium Distance L (Å) and the Corresponding MP2 Binding Energy (eV) of CO and H₂ on Different Sites of CNT Surfaces

Molecule	(A) hollow site		(B) bridge site		(C) surface site	
	L^b	E_b	L	E_b	L	E_b
CO-ext ^a	3.6	-0.124	3.2	-0.170	3.3	-0.161
CO-int	3.6	-0.159	3.2	-0.230	3.1	-0.195
H ₂ -ext	3.1	-0.068	3.1	-0.056	3.1	-0.060
H ₂ -int	3.1	-0.077	3.0	-0.083	2.8	-0.075

^a CO-ext denotes CO on the exterior CNT surface and H₂-int represents H₂ on the interior surface. ^b L : the equilibrium distance between the center of the adsorbed molecule and the CNT surface when the binding energy reaches the largest on that site.

the most stable E_b on site B is -0.170 eV at a much closer distance (3.2 Å) than on site A.

On the interior surface, the CO adsorption strength on different sites follows the same order as that on the exterior surface, but the binding energies are all higher than their exterior counterparts (Table 2). Thus, in general CO shows a stronger interaction with the interior CNT surface. In comparison to CO interacting with a planar graphite layer, the interaction strength decreases following interior CNT surface > planar graphite layer > exterior CNT surface, as shown in Figure 3a.

In comparison, H₂ adsorption is much weaker. For example, on the most favorable site A on the exterior CNT surface, the binding energy is only -0.068 eV , which agrees well with the values reported earlier from LDA calculations for the (5, 5) and (6, 6) CNTs.³⁸ However, it is much larger than those predicted for H₂ on the exterior (10, 0) and (9, 9) surfaces obtained with the generalized gradient approximation (GGA) method,^{22,23,39} which is known to underestimate the dispersion interactions between two molecules.

Inside the CNT, the adsorption strength of H₂ on different sites exhibits a different order from that on the exterior CNT surface. Site B is the most stable at $L = 3.0 \text{ Å}$. The binding energy (-0.083 eV) is higher than that on the most stable exterior site A, indicating a stronger attraction of H₂ inside the CNT. A similar trend is also observed for other models and the energy difference of H₂ adsorption on the interior and exterior CNT surface increases to -0.025 eV when a larger cluster model C₂₄H₁₂ and basis set 6-311++g (2df, 2pd) are used. Similar to CO, the binding energy of H₂ on CNT surfaces decreases in the order interior CNT surface > planar graphite layer > exterior CNT surface. This trend is consistent with an earlier study on the H₂ adsorption on the (10, 0) and (9, 0) CNTs within LDA and GGA,²³ as well as ab initio molecular-orbital theory computations inside and outside armchair and zigzag SWNTs.²¹

Different binding energies for H₂ and CO molecules on CNT surfaces can be explained by the nature of these molecules, the concave and convex geometries of the interior and exterior CNT surfaces and their particular electronic structures. Figure 4 shows the contour plots of the change in electron density ($\Delta\rho$) for H₂ and CO adsorbed on the interior and exterior surfaces of the (10, 10) CNT, where $\Delta\rho$ is defined as $\Delta\rho = \rho(\text{CNT} - \text{molecule})$

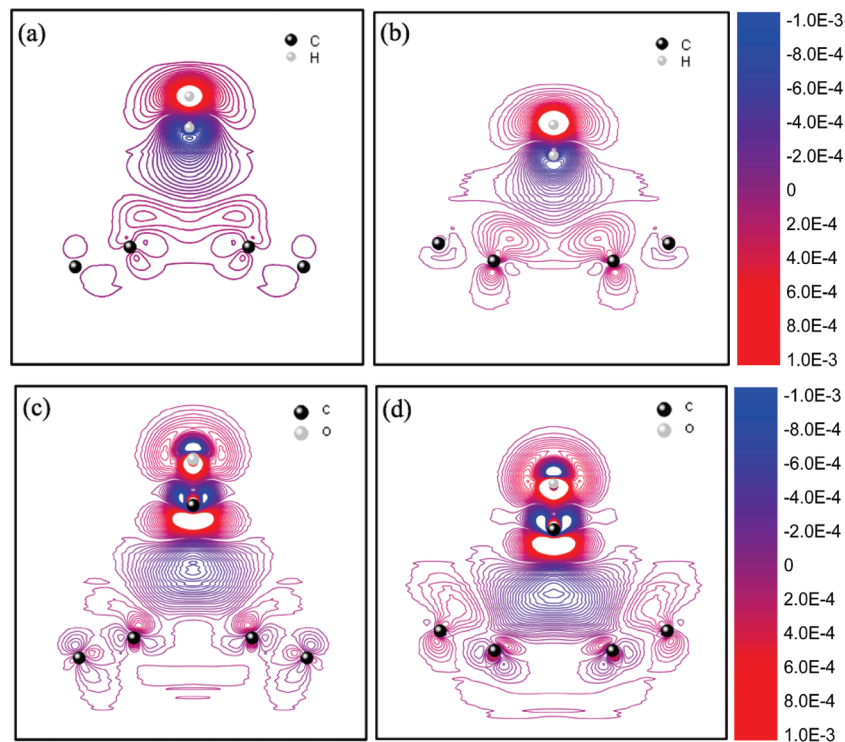


Figure 4. Contours of the change in electron density (a) H₂-ext; (b) H₂-int; (c) CO-ext, and (d) CO-int on site A of (10, 10) CNT surfaces. The carbon atoms of the nanotube are labeled by black balls. The area of the plot is 196 Bohr² and the unit of the scale bar is e/Bohr³. The red and blue contours indicate electron accumulation and depletion, respectively.

$-\rho(\text{CNT}) - \rho(\text{molecule})$. The change in electron density can demonstrate the interaction strength by illustrating the extent to which the electron density of both nanotube and the molecule are disturbed with respect to the independent nanotube and the molecule.²³

Figure S5b in Supporting Information shows the contour for the H₂ molecule on site A at a distance of 7 Å from the exterior CNT surface, indicating that there is almost no interaction. By contrast, when H₂ adsorbs at the equilibrium distance of 3.1 Å, the electron density is significantly redistributed (Figure 4a). One sees that electrons are shifted from the H atom near the CNT surface to the one far from the surface, resulting in an induced dipole. Figure 4b shows that the distortion of electron density becomes greater when H₂ adsorbs on the interior surface suggesting a stronger H₂-CNT interaction inside CNTs. This is consistent with the larger binding energy of H₂ inside the CNT (Table 2).

For comparison, we show in Figure 4c,d the contour maps of the change in electron density when CO adsorbs on the same CNT surface site as the H₂ molecule. The distortion of electron density is obviously greater in the CO-CNT than that in the H₂-CNT system, consistent with the higher binding energies of CO. Furthermore, the electronic structure is more perturbed if CO is inside the CNT. In addition, Figure S5c in Supporting Information also demonstrates that when CO adsorbs on the most stable site B, the electron redistribution is even more significant than on site A (Figure 4d). This is due to the dipole of the CO molecule and large polarizability of CNTs. A theoretical study carried out by Halls and Schlegel showed that [H₃NCH₃]⁺[Cl]⁻ ion pairs inside CNTs interact with the CNT wall via an induced image dipole on the nanotube and hence is stabilized.⁴⁰ Our calculations also show that the CO dipole induces an image dipole on the CNT surface when it adsorbs in configurations with the molecule axis parallel to the CNT surface, as shown in Figures S5c,d in Supporting Information.

Thus adsorption on sites B and C are more favored than on site A. The binding energy differs by ca. 0.071 eV between site B and A.

Since the curvature and electronic structure of CNTs vary with their diameters, the interactions of H₂ and CO molecules with CNT surfaces may also change. Therefore, we chose another two nanotubes with different diameters for comparison, that is, (7, 7) and (15, 15) CNTs. Their diameters are 9.49 and 20.34 Å, respectively, in comparison to 13.56 Å for the (10, 10) nanotube. Figure S6 in Supporting Information shows that the binding energies of H₂ and CO molecules on the exterior surface do not change significantly with the CNT diameter. However, inside CNT channels the interaction shows a much stronger dependence on the diameter. For example, the binding energies of H₂ increase with the decreasing CNT diameter. This is because hydrogen interacts with more near neighbor carbon atoms and the electronic structure is more perturbed when the CNT surface contracts. However, CO adsorption inside CNTs does not appear to follow a simple trend. The binding energy on the interior (10, 10) surface is larger than that on the (15, 15) tube, as expected. However, it is weaker inside the (7, 7) tube relative to the (10, 10) tube. This may be because the repulsive component of the LJ potential becomes dominant due to overlap of the CO and CNT orbitals inside the small tube (7, 7), as suggested by an earlier study.⁷ Thus there is an optimum diameter of CNT for stable adsorption of a given molecule.⁷ It can also be seen from Figure S6 in Supporting Information that the binding energy difference between the interior and exterior surfaces generally becomes larger for smaller nanotubes.

3.2. Local Concentrations of H₂ and CO Molecules Inside and Outside of CNTs. The local concentrations of CO and H₂ molecules inside and outside of CNTs were calculated using the potential parameters obtained from first-principles calculations (Tables 1, and S3 and S4 in Supporting Information). Figures 5a and S7a in Supporting Information show that the

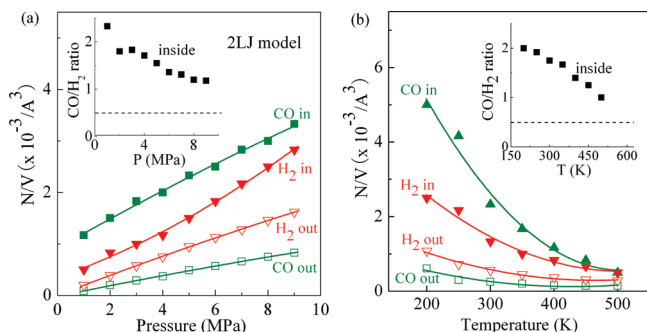


Figure 5. Concentrations of CO and H₂ molecules inside and outside of a (10, 10)-(13, 13) DWNT as a function of (a) pressure and (b) temperature obtained with the 2LJ model. The inserts show the ratio of CO/H₂ inside the CNT (filled squares) in comparison to the ratio in the gas phase (dashed lines).

inside concentrations of CO and H₂ molecules are higher than the outside ones in the pressure range of 1–9 MPa using either the 2LJ or the 3LJ model. This suggests that molecules are enriched inside nanotubes. The slightly lower concentrations from the 3LJ model than those from the 2LJ model may be due to the smaller ϵ_{CS} in CO-nanotube interaction potentials. More interestingly, the CO enrichment is higher than that of H₂ inside CNTs, resulting in a CO/H₂ ratio higher than 0.5 in the exterior gas phase, represented by the dashed line in the insert of Figure 5a. The enrichment of syngas inside CNTs can be explained by the stronger interaction of H₂ and CO with the interior CNT surface, and the stronger attraction of CO relative to H₂ leads to the preferred adsorption of CO inside CNTs. With increasing pressure this CO segregation becomes weaker although the concentrations of both CO and H₂ further increase inside CNTs. For example, the CO/H₂ ratio is 2.33 at 1 MPa but decreases to 1.18 at 9 MPa. This is possibly due to the smaller molecule size of H₂ compared to CO. More H₂ than CO can squeeze into CNT channels at higher pressures, which lowers the ratio of CO/H₂. Jiang et al. studied the adsorption of a N₂/O₂ mixture on CNTs and also observed that smaller molecules enter the nanotube channel preferably at high pressures.¹⁴ A higher concentration of H₂ and CO is also observed in (10, 10) CNT calculated using the LJ potentials of the planar graphite layer (Figure S7b in Supporting Information), which can be simply attributed to the space restriction of the nanochannels. However, the enrichment is much weaker than the case where the electronic structure is considered in the 2LJ model.

Figure 5b shows that the concentrations of both molecules whether inside and outside of CNTs decrease with the temperature. Furthermore, the CO concentration inside nanotubes decreases much more dramatically, resulting in a declining ratio of CO/H₂. This indicates that both the enrichment of syngas molecules and the segregation of CO inside CNTs against the gas phase composition are more significant at lower temperatures. But the interior CO/H₂ ratio remains higher than that in the gas phase up to 573 K, which is in the temperature range for syngas conversion to liquid fuels and oxygenates.

Figure S8 in Supporting Information shows that both H₂ and CO are more enriched inside smaller nanotubes at lower pressures. However, with the pressure increasing above 4 MPa, the concentrations inside (7, 7) level off. This can be attributed to the spatial restriction of very small nanochannels, which prohibits further entry of more molecules. In comparison, inside larger tubes, for example, (10, 10) and (15, 15), this space limit comes at a higher pressure and the concentrations of syngas increase just monotonically up to 9 MPa. Figure 6 demonstrates

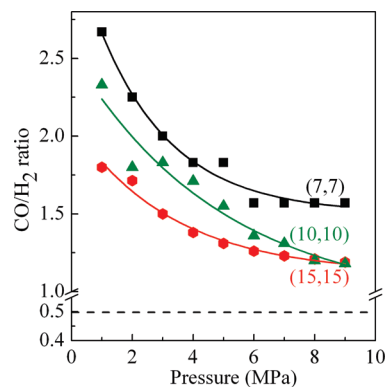


Figure 6. Ratio of CO/H₂ inside CNTs with different diameters as a function of pressure. The dashed line indicates the ratio of CO/H₂ (0.5) in the gas phase.

that the CO/H₂ ratio inside (7, 7) and (15, 15) CNTs also declines with pressure, similar to that in the (10, 10) CNT. More importantly, the CO/H₂ ratio increases with decreasing diameter of CNTs, suggesting that segregation of CO against the exterior gas phase composition becomes more significant inside smaller nanotubes. A higher concentration of reactants could lead to a faster reaction rate. Moreover, the altered ratio of CO/H₂ hints at the possibility of tuning the product selectivity through confinement inside CNTs.

4. Conclusion

The nanochannels formed by curved graphene layers in carbon nanotubes provide an interesting confinement environment for chemical reactions. This theoretical study shows that both H₂ and CO molecules are enriched inside CNT channels with respect to those on the outside. The enrichment generally becomes more significant inside smaller nanotubes at lower temperatures and higher pressures. In the presence of CO/H₂ (volume ratio 0.5) mixture, CO is preferentially enriched inside CNTs resulting in a notably higher CO/H₂ ratio compared to that on the outside of CNTs. This enrichment of molecules and altered ratio of CO/H₂ may provide a novel approach to tune the reaction rate and product selectivity by confining the reaction inside CNTs. However, a reaction in the presence of metal catalyst particles inside CNT channels involves multiple interactions among reactant molecules, products, CNT walls, and catalyst surfaces, as well as the transport behavior of reactants and products in CNTs. Therefore, further studies are needed to elucidate the effect of confining catalysts inside CNTs and consequent catalytic reactions over such confined catalysts.

Acknowledgment. We thank Professor Weixue Li from Dalian Institute of Chemical Physics, Professor Jijun Zhao from Dalian University of Technology, and Professor Zhaoxu Chen from Nanjing University for discussions. The authors acknowledge the financial support from the National Natural Science Foundation of China (Project Nos. 20503033 and 20573107) and the Ministry of Science and Technology of China (Project Nos. 2005CB221403 and 2006CB932703).

Supporting Information Available: The choice of basis set, LJ potential parameters for H₂ and CO interacting with graphite and CNTs, comparisons of the interactions of H₂-CNT and CO-CNT using different methods, the influence of the interior (13, 13) potentials on the interactions of molecules-interior (10, 10) surface, the MP2 binding energies of H₂ and CO on different sites of a (10, 10) CNT, differential electron density of molecule-

CNT, the MP2 binding energies as a function of CNT diameters, the concentrations of CO and H₂ molecules obtained with the potential parameters of the 3LJ model and graphite, and local concentrations of CO and H₂ molecules versus CNT diameters. This material is available free of charge via the Internet at <http://pubs.acs.org>.

References and Notes

- (1) Dai, H. *Acc. Chem. Res.* **2002**, *35*, 1035.
- (2) Baughman, R. H.; Zakhidov, A. A.; de Heer, W. A. *Science* **2002**, *297*, 787.
- (3) Avouris, P. *Acc. Chem. Res.* **2002**, *35*, 1026.
- (4) Kondratyuk, P. P.; Yates, J. T. *Acc. Chem. Res.* **2007**, *40*, 995.
- (5) Koga, K.; Gao, G. T.; Tanaka, H.; Zeng, X. C. *Nature* **2001**, *412*, 802.
- (6) Smith, B. W.; Monthieux, M.; Luzzi, D. E. *Nature* **1998**, *396*, 323.
- (7) Britz, D. A.; Khlobystov, A. N. *Chem. Soc. Rev.* **2006**, *35*, 637.
- (8) Chen, W.; Pan, X. L.; Bao, X. H. *J. Am. Chem. Soc.* **2007**, *129*, 7421.
- (9) Chen, W.; Pan, X. L.; Willinger, M. G.; Su, D. S. *J. Am. Chem. Soc.* **2006**, *128*, 3136.
- (10) Pan, X. L.; Fan, Z. L.; Chen, W.; Ding, Y. J.; Luo, H. Y.; Bao, X. H. *Nat. Mater.* **2007**, *6*, 507.
- (11) Chen, W.; Fan, Z. L.; Pan, X. L.; Bao, X. H. *J. Am. Chem. Soc.* **2008**, *130*, 9414.
- (12) Pan, X. L.; Bao, X. H. *Chem. Commun.* **2008**, 6271.
- (13) Santiso, E. E.; George, A. M.; Turner, C. H.; Kostov, M. K.; Gubbins, K. E.; Buongiorno-Nardelli, M.; Sliwinski-Bartkowiak, M. *Appl. Surf. Sci.* **2005**, *252*, 766.
- (14) Jiang, J.; Sandler, S. I. *Langmuir* **2004**, *20*, 10910.
- (15) Darkrim, F.; Levesque, D. *J. Chem. Phys.* **1998**, *109*, 4981.
- (16) Shi, W.; Johnson, J. K. *Phys. Rev. Lett.* **2003**, *91*, 015504.
- (17) Kostov, M. K.; Cheng, H.; Cooper, A. C.; Pez, G. P. *Phys. Rev. Lett.* **2002**, *89*, 146105.
- (18) Haddon, R. C. *Science* **1993**, *261*, 1545.
- (19) Zhao, J. J.; Buldum, A.; Lu, J. P. *Nanotechnology* **2002**, *13*, 195.
- (20) Barone, V.; Heyd, J.; Scuseria, G. E. *J. Chem. Phys.* **2004**, *120*, 7169.
- (21) Ferre-Vilaplana, A. *J. Chem. Phys.* **2005**, *122*, 214724.
- (22) Han, S. S.; Lee, H. M. *Carbon* **2004**, *42*, 2169.
- (23) Henwood, D.; Carey, J. D. *Phys. Rev. B* **2007**, *75*, 245413.
- (24) Tada, K.; Furuya, S.; Watanabe, K. *Phys. Rev. B* **2001**, *63*, 155405.
- (25) Dillon, A. C.; Jones, K. M.; Bekkedahl, T. A.; Kiang, C. H.; Bethune, D. S.; Heben, M. J. *Nature* **1997**, *386*, 377.
- (26) Liu, C.; Fan, Y. Y.; Liu, M.; Cong, H. T.; Cheng, H. M.; Dresselhaus, M. S. *Science* **1999**, *286*, 1127.
- (27) Gu, C.; Gao, G. H.; Yu, Y. X.; Nitta, T. *Fluid Phase Equilib.* **2002**, *194*, 297.
- (28) Frisch, M. J.; Trucks, G. W.; Schlegel, H. B.; et al. *Gaussian98*, revision A.9; Gaussian, Inc.: Pittsburgh, PA, 1998.
- (29) Okamoto, Y.; Miyamoto, Y. *J. Phys. Chem. B* **2001**, *105*, 3470.
- (30) Ferre-Vilaplana, A. *J. Chem. Phys.* **2005**, *122*, 104709.
- (31) Heine, T.; Zhechkov, L.; Seifert, G. *Phys. Chem. Chem. Phys.* **2004**, *6*, 980.
- (32) Bojan, M. J.; Steele, W. A. *Langmuir* **1987**, *3*, 116.
- (33) Straub, J. E.; Karplus, M. *Chem. Phys.* **1991**, *158*, 221.
- (34) Piper, J.; Morrison, J. A.; Peters, C. *Mol. Phys.* **1984**, *53*, 1463.
- (35) *CERIUS 2*, Version 4.2; Molecular Simulations Inc.: San Diego, CA, 2000.
- (36) According to our first-principle calculations, the binding energies of H₂ and CO on the most stable site of exterior (13, 13) CNT are -0.070 and -0.177 eV, respectively, which are close to the corresponding values on the exterior CNT (10, 10), that is, -0.068 and -0.170 eV. Thus, it is reasonable to use the potential parameters of the exterior (10, 10) to model the outside (13, 13) tube.
- (37) Santucci, S.; Picozzi, S.; Di Gregorio, F.; Lozzi, L.; Cantalini, C.; Valentini, L.; Kenny, J. M. *J. Chem. Phys.* **2003**, *119*, 10904.
- (38) Arellano, J. S.; Molina, L. M.; Rubio, A. M.; López, J.; Alonso, J. A. *J. Chem. Phys.* **2002**, *117*, 2281.
- (39) Mpourmpakis, G.; Froudakis, G. E.; Lithoxoos, G. P.; Samios, J. *J. Chem. Phys.* **2007**, *126*, 144704.
- (40) Halls, M. D.; Schlegel, H. B. *J. Phys. Chem. B* **2002**, *106*, 1921.

JP906092C